Characterization of the Human Body Impact on UAV-to-Ground Channels at Ultra-Low Altitudes

Mahmoud Badi, Sabyasachi Gupta, Dinesh Rajan, *Senior Member, IEEE*, and Joseph Camp, *Member, IEEE*

***Abstract*—At ultra-low altitudes, an unmanned aerial vehicle (UAV) can act as a personal base station where it communicates only with one user. User equipment (UE) can be inside the pocket of a user or near their chest while facing or facing-away from the flying base station. In these scenarios, the wireless channel can go through different fading levels, depending on the UAV's location, user orientation, the location of the UE near the user's body, and the frequency of the transmitted signal. In this work, we provide measurement results and investigate how the human body affects the Air-to-Ground (AtG) channel characteristics under various use cases of holding a device. These channel characteristics include the average signal strength, shadowing, multipath, and the Rician K-factor. We target three different use cases of holding the device: Near-Chest Facing, In-pocket Facing, and Near-Chest Facing-away from the transmitting UAV. We perform this study at carrier frequencies of 900 MHz and 2.5 GHz and in Line-of-Sight conditions. First, we conduct a set of baseline experiments to understand ground-to-ground and AtG channels in free space. Second, we conduct AtG experiments with the user holding the device and show that the human body can induce either gains or losses compared to free space, depending on its relative orientation to the UAV. Third, we find that there are two distinct regions of operation, one in which the channel characteristics are mainly affected by the UAV and another that is dominated by the user's body. Fourth, we address the time-varying nature of the K-factor and analyze the user's body impact on its mean and standard deviation. We find that if a user changes their orientation to face away from the transmitting UAV, their body can cause extreme fluctuations in the K-factor value over time and reduce its mean value by an average and a maximum of 6.8 and 15 dB, respectively. Finally, to demonstrate the impact of our findings on the design of deployment strategies of UAVs, we considered how the human body and the relative UAV hovering position can affect the physical layer security in a UAV-assisted network. We show that the secrecy rate for a UAV-based network can be heavily influenced by the human body orientation relative to the UAV hovering location, consequently resulting in a different optimal deployment strategy compared to existing schemes that employ free-space pathloss models that neglect such human-induced effects.**

***Index Terms*—Air-to-Ground channels, Human body effects, Physical layer security, UAV body effects.**

Manuscript received September 15, 2021; accepted September 26, 2021. Date of publication October 26, 2021; date of current version January 20, 2022. This work was supported in part by the NSF via Grants CNS-1823304 and CNS-1909381 and in part by the Air Force Office of Scientific Research via under Grant FA9550-19-1-0375. Part of this work has been accepted at IEEE MILCOM, San Diego, CA, USA, December 2021 [1]. The review of this article was coordinated by Prof. Khoa Le. *(Corresponding author: Mahmoud Badi.)*

The authors are with the Department Electrical and Computer Engineering, Southern Methodist University, Dallas TX 75275 USA (e-mail: mbadi@smu.edu; sabyasachig@smu.edu; rajand@smu.edu; camp@smu.edu).

Digital Object Identifier 10.1109/TVT.2021.3122413

I. Introduction

DUE to features such as being lightweight, affordable, and having three-dimensional (3D) maneuverability, unmanned aerial vehicles (UAVs) are becoming more ubiquitous than ever. With UAVs being integrated in applications such as entertainment, inspection, smart agriculture, delivery, and emergency rescue [1]–[3], their global market value is expected to reach $43 billion by 2025 [4]. In many applications, UAVs might need to communicate with a device that is either being held or attached to a person at altitudes close to the ground. A person can be holding user equipment (UE) near their chest or in their pocket while downloading or uploading data. Moreover, the direction of the user relative to the UAVs can take on any arbitrary value. For example, a user could be texting (holding the UE near their chest with both hands) while facing the UAV or facing-away from it. Due to these different use cases, the wireless channel might go through dramatic changes [7], [8]. Consequently, the optimal placement of the UAVs, which targets, say, the highest achievable throughput or minimum energy consumption, depends on the near-body location (near chest or in pocket) or user direction (facing or facing-away). Moreover, due to user-antenna interaction, antenna radiation patterns can be altered and significant variations in the received signal can be experienced by the user [12], [14], [21]. Such effects can be observed even in the case of facing a transmitter while holding a device with different grips and/or postures [15], [20]. While the role of the human body and its effects on terrestrial wireless channels has been the focus of many works, the impact of the user-induced effects on UAV-to-ground[1] channels has been mostly disregarded in literature. The uniqueness of this case study comes from the ability of UAVs to adjust their position in 3D space based on the observed use case. We show that factors such as UE location and user orientation along with the UAV's 3D location and its antenna radiation pattern have a considerable impact on the wireless channel. In addition, simulation and optimization models, which constitute the majority of UAV-related work, such as [38], [41], do not consider such human-related factors. Therefore, measurement campaigns that target this issue are necessary.

In this work, we investigate how three different use cases of holding a communication device, namely, near-chest

[1]We use Air-to-Ground and UAV-to-ground interchangeably.

facing (NCF), in-pocket facing (IPF), and near-chest facing-away (NCFA), can affect the UAV-to-ground channel at ultra-low altitudes (less than 30 m altitude). We measure and analyze how the average received signal strength (RSS), shadowing, and small-scale fading are affected by the UAV hovering position, user orientation, and the UE near-body location. We then quantify how the observed effects can impact real-world applications such as physical layer security of a UAV-assisted network. We target two carrier frequencies, 900 MHz and 2.5 GHz, both of which have many narrowband Internet-of-Things (IoT) based applications such as IEEE 802.15.4 technology [5] as well as broadband services [6]. To the best of our knowledge, this is the first study to measure and quantify how the human body and user behavior can impact the UAV-to-ground channel at various drone locations. The conclusions presented here are the results of the thorough analysis of 144 datasets spanning 18 different drone hovering locations, three different use cases, and two carrier frequencies, in addition to free-space baseline experiments. Our contributions can be summarized as follows:

- We show that, compared to a baseline user-free (free-space) scenario, the existence of the human body near a UE can result in increased or decreased RSS levels, depending on the user's orientation. These user-induced "gains", or "losses" are found to depend on the frequency used and the UAV's hovering position.
- We experimentally demonstrate how the UAV's hovering position and user orientation can affect shadowing and multipath in ultra-low LOS UAV-to-Ground channels. We quantify their effect and show that, except for one drone hovering position at which the UAV's body dominates influence on the channel, shadowing, multipath, and the Rician K-factor strongly depend on the user body orientation, not the UAV's body nor its location.
- We show that, while moving the UE from near the chest to inside the pocket could lead to some degradation in channel quality, improvements could be achieved by simply readjusting the drone's hovering altitude. We explain how these improvements relate to the elevation radiation pattern of the antenna, traveled distance, and clearance from the UAV body.
- We address the time-varying nature of the K-factor as a result of UAV hovering and relative direction of the user. Then, we show that, except for one drone hovering position, the user's body could lead to significant degradation in the K-factor reducing it by an average and a maximum of 6.8 dB and 15 dB, respectively. Frequency comparison is then performed revealing that the K-factor at 900 MHz is higher than 2.5 GHz across all use cases.
- To highlight the impact of our findings, we propose an application in which the obtained insight could be valuable for the case of physical layer security in UAV-assisted networks. We have shown that a significant improvement in physical layer security performance for a UAV assisted network can be achieved when the hovering locations of the UAVs are decided considering users' orientations and their body effect.

This paper is organized as follows. In Section II, we present some background knowledge and discuss related work. In Section III, we present our experimental setup and the channel model. Experiment procedures and calibration are discussed in Section IV. The baseline (user-free) results are presented in Section V. User impact on the UAV-to-ground channel is discussed in Sections VI and VII. The impact of our findings on one UAV-based application is demonstrated in Section VIII, and conclusions are presented in Section IX.

II. Background Knowledge and Related Work

First, we briefly review the basic mechanisms of signal propagation through the human body. Then, we discuss literature related to the two main topics involved in this work.

A. Background: Propagation Through the Human Body

The human body absorbs and reflects electromagnetic energy. At the air-human interface, some energy will be reflected, depending on the refraction index or the intrinsic impedance, both of which are a function of the permeability and permittivity of human body tissue [18], [19], which is frequency dependent. Another part of the signal will penetrate through the body's multiple layers, experiencing attenuation mainly due to absorption and multipath reflections within the tissues. Attenuation due to absorption and propagating through the human body is exponential with respect to the thickness of the body and has been shown to be the main contributor to electromagnetic energy loss with values reaching up to 35 dB [22]. The amount of attenuation due to absorption has been shown to considerably vary with frequency and the tissue thickness [19], [21] with visceral fat being the dominant tissue type in determining the loss. Finally, after many reflections/transmissions within the body's many layers, the remaining part of the signal will leave the human body and propagates back into the air.

B. Related Work

We classify related literature into two main bodies of work. The first deals with human-based communications, while the second studies UAV Air-to-Ground channels at low or ultra-low altitudes.

Human-Induced Effects: The impact of the human body on the wireless channel has been the focus of many studies. The human body as an antenna was investigated in [10], and the results showed that the human body could increase signal reception and that the reflection coefficient could be improved by different human body postures. The human body interaction with devices and its use as an antenna was leveraged in [11] in building a system that can recognize gestures. The work in [12] showed that the human body can significantly alter the effective radiation pattern of the antenna at 2.4 GHz. In addition, losses of up to 25 dB were found due to blockage from the human body. A similar finding of 21 dB loss at the same frequency was reported in [9]. In [20], an average loss of 20 dB was recorded due to covering a mobile device antenna with the hand. In [15], it was shown that the body of the user, when facing a transmitter at millimeter wave frequencies, can actually contribute to the radiation of the antenna and result in higher received signal levels compared to free-space scenarios.

A similar finding was reported in [8], where four different frequencies were investigated for a user facing and facing-away from a ground transmitter. User-induced effects on shadowing were investigated at 2.45 GHz in stationary, rotating, and mobile scenarios in [17]. This study revealed that when a user, who is holding a highly-directional patch antenna, obstructs the signal path, significant reductions in RSS levels were measured. The variation in RF losses within the human body at two frequencies (403 MHz and 923 MHz) was investigated in [19]. It was shown that the RF transmission loss within the human body is higher at the lower frequency and that the results varied depending on the thickness of the tissues, especially the visceral fat. The work in [21] investigated the impact of three different human body types on radiated power at 17 different frequencies. The results showed that at high frequencies, gains compared to free space could be achieved. The work also highlighted how the radiated and absorbed power vary with body type. In [13] pathloss for eight different human body sizes was investigated and the results showed a variation of up to 13 dB in pathloss and 21% in pathloss exponent due to the different body sizes. A statistical channel model was developed in [16] to capture the effects of a person walking in two different directions relative to a transmitter with a device attached to their wrist. A study that investigates on-body communications for a wide range of frequencies (420 MHz to 2.4 GHz) and technologies was conducted in [23]. The impact of a user's head and hand on antenna radiation pattern at 880 MHz was studied in [7], and it was shown that user-antenna interaction can alter both the magnitude and phase of the antenna radiation pattern. Leveraging the strong multipath effects experienced within the body tissues, the work in [22] used signals with different frequencies to achieve beamforming at a target placed within the tissue of an animal. A machine learning approach that utilizes received signal strength to distinguish between different user modes at millimeter wave frequencies was proposed in [43].

UAV-to-Ground Studies: The work in [24] studies a UAV-to-Ground channel at ultra-low altitudes for three different environments and two user modes: texting and calling. Measurements and analysis were carried out for a limited drone path of 20 m with an emphasis on the impact of the environment on the channel rather than the human body. The work in [26] experimentally characterizes large-scale fading components in drone-to-ground channels, where the ground node was mounted on a tripod. The work in [31] characterized the K-factor for low-altitude UAVs in urban environments crowded with buildings and spanned large horizontal distances. Channel characterization of wideband AtG channels in different environments was carried out in [34]. Low altitude UAV AtG channels for a wide range of frequencies (1 to 24 GHz) were experimentally studies in [35], [36]. The feasibility of using a drone-based channel sounding method for a cell-free massive MIMO setup was recently demonstrated in [32]; in this work, the channel between the drone and four ground UEs – that were not held by humans – was studied. The AtG channel was measured for four different UEs on the ground, and the SNR and channel gain were analyzed for different UAV heights. Another AtG sounding method for millimeter wave channels was demonstrated in [28]. In [25], autonomous QoS-driven UAVs in UAV-to-ground channels are prototyped and experimentally investigated for three ground devices that were not held by humans. Our previous work [29] investigated how the drone body and antenna orientation can affect ground-to-UAV channels at ultra-low altitudes but without human involvement. Distributed beamforming from a UAV swarm to a ground node that was mounted on a platform was experimentally demonstrated in [27]. The work in [33] demonstrated a UAV that can change its hovering location based on changes in the wireless channel that were caused by a user holding a UE. However, the impact of the human body was not considered and movement decisions were predefined. In addition to the aforementioned works, there exists many studies that investigate the optimal deployment and trajectory optimization of UAVs in AtG channels such as [38]–[40], [42]. However, these works do not consider the human-induced effects, which could be substantial, as we demonstrate in this work.

While the above two bodies of work provide valuable insight when it comes to either field, studies that bridge the gap between the two are still missing. This is what we attempt through this work. Specifically, our study provides an understanding of how the human body can influence such channels with various use cases and considering many UAV hovering positions and frequencies. We believe that although only considering the user and UAV might not be enough to fully understand all the intricate details of such channels, the ability to measure and characterize the relative impact is key into moving forward with more realistic channel models and algorithms that take the human body into account.

III. System Description and Channel Model

In this section, we present our hardware and software setup. Then, we discuss the signal and channel models and present the measurement environment.

A. Hardware and Software Setup

Two of the Universal Software Radio Peripheral (USRP) E312 s from Ettus Research$^{\mathrm{TM}}$ are configured for collecting measurements. The transmitting radio is mounted on a tripod in the baseline ground-to-ground (GtG) experiments and on the UAV in the Air-to-Ground (AtG) experiments. The transmitting antenna is vertically mounted, oriented upward and is directly connected to the TRX port using an SMB to SMA adapter. The receiver USRP is either mounted on a tripod, such as the case in the user-free GtG and AtG experiments, or being held by the user, which is the case in the human-related experiments. Both radios utilize omni-directional, linearly-polarized antennas (Ettus VERT2450) with a radiation pattern in the azimuth and elevation planes, as shown in Figs. 2(b) and 2(c). The transmitter is configured to send an unmodulated carrier at a sampling rate of 64-thousand samples/second. The receiver, sampling at the same rate, is configured to write the received IQ samples to a binary data file as complex floating point numbers. Measurements are recorded for a period of 20 seconds per hovering/Rx location. The processing and analysis is conducted over the middle 15 seconds to ensure the exclusion of the unwanted drone transition effects that might occur when the UAV is moving toward or away

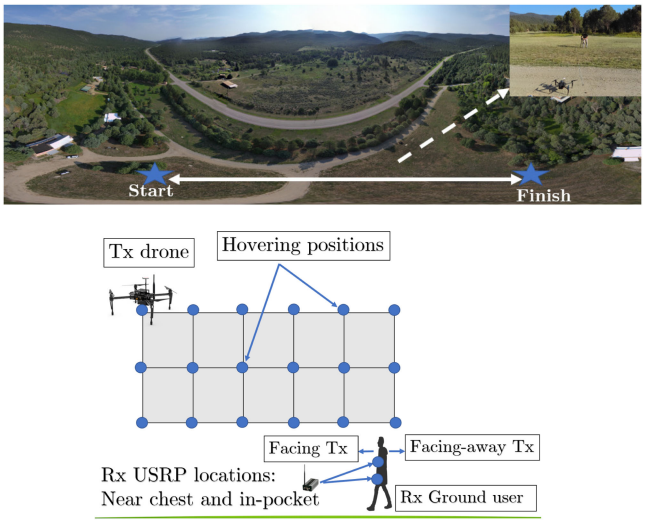

Fig. 1. Aerial view of the experiment location and an illustration of the investigated user orientations and UAV locations.

from the desired location. The absolute value of the complex envelope is then used for further postprocessing.

B. Signal Model

We use an unmodulated continuous wave (CW) transmission. The transmitted signal is $x(t) = \cos(2\pi f_c t + \phi_o)$, where f_c is the carrier frequency generated by the local oscillator (2.5 GHz or 900 MHz) with a phase offset of ϕ_o. When the transmitted signal passes through the wireless channel, which is a linear time-invariant (LTI) system, the received signal will be a scaled and phase-shifted version of the transmitted signal. Due to multipath reflections coming from the UAV body effects [29] and ground reflections, multiple components will interact at the receiver, resulting in constructive and destructive interference. The received signal can be written as [46]:

$$r(t) = \Re\left\{\left[\sum_{n=0}^{N(t)} \alpha_n(t) e^{-j\Phi_n(t)}\right] e^{j2\pi f_c t}\right\} \tag{1}$$

Here, $N(t)$ is the number of multipath components, and the phase term Φ is given by $\Phi_n(t) = 2\pi f_c \tau_n(t) - \phi_{D_n} - \phi_o$. The propagation delay of the n^{th} component is represented by τ_n, which is equal to $d_n(t)/c$ with $d_n(t)$ being the separation distance in meters and c being the speed of light; $\alpha_n(t)$ is the amplitude of the n^{th} multipath component, and ϕ_{D_n} is the Doppler shift. In terms of in-phase and quadrature components, we can rewrite the received signal as:

$$r(t) = r_I(t)\cos(2\pi f_c t) + r_Q(t)\sin(2\pi f_c t) \tag{2}$$

Here, $r_I(t) = \sum_{n=0}^{N(t)} \alpha_n(t)\cos\Phi_n(t)$ and $r_Q(t) = \sum_{n=0}^{N(t)} \alpha_n(t)\sin\Phi_n(t)$ are the in-phase and quadrature components, respectively. After quadrature demodulation and low-pass filtering, assuming there is no carrier frequency offset (CFO), the received signal at baseband (which is used for actual processing) has the complex magnitude of:

$$|r(t)| = \sqrt{r_I^2(t) + r_Q^2(t)} \tag{3}$$

As we can see, the received signal envelope is not constant. Given that Doppler effect is negligible when hovering, the received signal envelope will vary over time, depending mainly on multipath reflections and fluctuations in the separation distance, which is caused by the continuous hovering motion of the UAV. In addition, the human body location involved in the signal path will result in attenuation and cause multipath effects. For instance, when facing-away, the amount of attenuation will be significantly greater than when in the pocket and the signal will experience more multipath effects as it passes through the human body tissues [22].

Next, we explain the statistical distribution of the channel model and how the samples are processed.

C. Channel Model and Signal Analysis

In our experiments, the channel is assumed to consist of a direct line-of-sight (LOS) component, which might be exposed to different shadowing levels. The channel also consists of multipath components that can constructively or destructively interfere with the direct component, resulting in fast signal fluctuations. As a result, the received complex envelope is made up of the complex sum of two phasors, the direct path, and a construction of multiple paths, resulting in a Rician distributed envelope [46]. Hence, the channel is assumed to have a Rician distribution and characterized accordingly. The Rician probability density function is given by [46]:

$$f(r) = \frac{r}{\sigma^2}\exp\left(-\frac{r^2+a^2}{2\sigma^2}\right) I_o\left(\frac{ra}{\sigma^2}\right), r \geq 0 \tag{4}$$

Here, a represents the amplitude of the direct component, $2\sigma^2$ is the average power of the multipath components, and I_o is the Bessel function of the zeroth order. The parameters of the Rician distribution are obtained through the Method of Moments approach [47]. The moments here are the mean and standard deviation of the power p, which is obtained through squaring the normalized absolute value of the complex envelope (*i.e.*, $p = r^2$). Then, we obtain the mean and standard deviation of the power over a time duration window of 4000 samples (*i.e.*, 62.5 ms). The window size is found to satisfy the trade-off between the desire to analyze the shortest time duration possible, to capture small-scale fluctuations, while still remaining statistically meaningful. A similar window size was chosen in our previous work [29]. The windowed mean and standard deviation of power are denoted as $\mu = mean(W(p_n))$ and $\eta = std(W(p_n))$, where W is the windowing operation [30]. From μ and η, we can then calculate the Rician distribution parameters for the considered window as follows: $a^2 = \sqrt{\mu^2 - \eta^2}$, $2\sigma^2 = \mu - \sqrt{\mu^2 - \eta^2}$. The Rician K-factor per window is then calculated as:

$$K(dB) = 10\log_{10}\left[\frac{a^2}{2\sigma^2}\right] \tag{5}$$

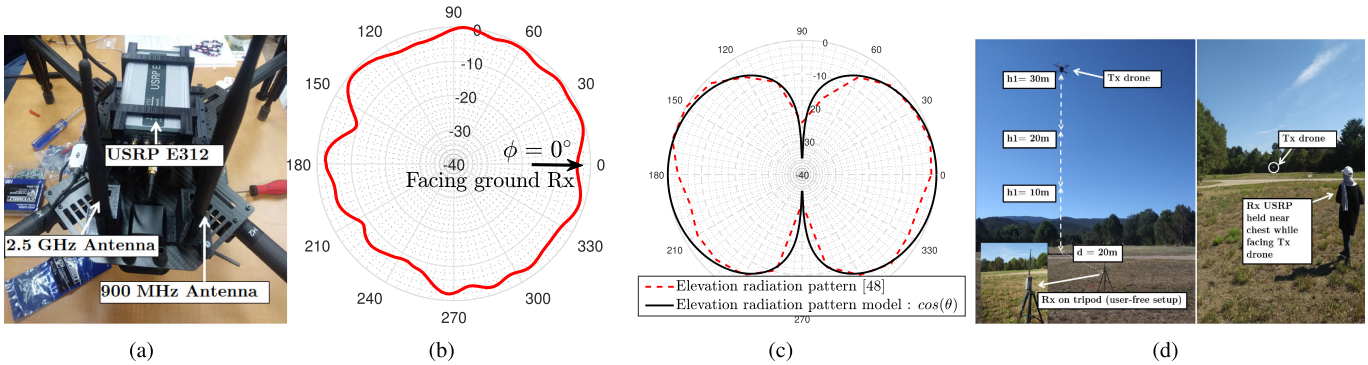

(a) (b) (c) (d)

Fig. 2. (a) The UAV platform with the used antennas at 2.5 GHz and 900 MHz. (b) Azimuth and (c) elevation radiation pattern of the antenna at 2.5 GHz. (d) Location and setup for the UAV-to-Ground experiments. The user-free (no human body involvement) setup (left) and NCF setup (right) are shown.

Recall that $K = -\infty$ dB indicates the absence of a dominant LOS component, resulting in a Rayleigh channel.

D. Measurement Environment

The experiments were conducted in the SMU-in-Taos campus in Taos, New Mexico. The location is shown in Fig. 1. The experiment path (depicted by the white arrow) is clear from any obstacles, *i.e.,* no trees, buildings, or cars. The surrounding environment, which constituted mostly of trees, was monitored to make sure that no moving objects existed throughout the experiments. The frequency spectrum was continuously monitored to make sure there were no interfering transmissions.

IV. Experiments Procedure and Calibration

We conducted three sets of experiments: User-free Ground-to-Ground, User-free UAV-to-Ground, and UAV-to-Ground with different UE use cases. In the following section, we explain the procedure of each of these experiment sets.

A. User-Free Ground-to-Ground Channels

To construct a baseline understanding of pathloss and the surrounding environment, we conduct Ground-to-Ground (GtG) measurements at carrier frequencies 900 MHz and 2.5 GHz. Here, the only variable is the horizontal distance between the transmitter and receiver. Both nodes are mounted on a tripod 1.5 m above ground (see Fig. 2(d) for one tripod location), and measurements take place at six horizontal distances of $d_1 = 0$ m (Rx next to Tx), $d_2 = 20$ m, $d_3 = 40$ m, $d_4 = 60$ m, $d_5 = 80$ m, and $d_6 = 100$ m.

B. User-Free UAV-to-Ground Channels

With the same receiver (Rx) still on the tripod, the transmitter (Tx) is now mounted on the UAV. The Tx UAV visits the same previous Tx locations (same horizontal distances) at three different altitudes from the ground: $h_1 = 10$ m, $h_2 = 20$ m, and $h_3 = 30$ m. See Fig. 2(d) for a depiction of the altitudes and experiment location. If we denote one location by its horizontal distance (d) and altitude (h), then to describe, for example, the Tx UAV location at the fifth horizontal distance (80 m) and third altitude (30 m), we use the notation of (d_5, h_3).

Measurement collection starts when the UAV hovers above the user at d_1 and altitude h_1. Then, the UAV changes its horizontal distance from d_1 to d_2 and measurements are collected again. The process is repeated until the UAV reaches d_6 for the same altitude, h_1. The UAV then moves to h_2 and the process is repeated until all hovering positions are covered, ending with (d_6, h_3). Fig. 1 shows the hovering positions.

C. UAV-to-Ground Channels With Different UE Use Cases

Here, we repeat the previous measurements but with a user holding the UE (Rx USRP). The weight and height of the human subject are approximately 56 kg and 164 cm. We investigate three use cases: (*i*) Near chest and facing (NCF) the Tx UAV, (*ii*) Near chest and facing-away (NCFA) from the Tx UAV, and (*iii*) In-pocket while facing (IPF) the Tx UAV. For each use case, we perform AtG experiments at carrier frequencies of 900 MHz and 2.5 GHz, totalling 6 experiment sets. In each of these experiment sets, we analyze how the RSS levels, shadowing, and the Rician K-factor are affected by user orientation, UE near-body location, and the drone's hovering position. An illustration of when a user is facing the Tx UAV while holding the radio device with two hands is shown in Fig. 2(d).

D. Power Calibration With USRP E312

We performed a calibration of the transmit power at various gains for both frequencies. The term gain here refers to the RF chain gain within the USRP, which comes from the power amplifier and other components within the device's circuit. The calibration setup is shown in Fig. 3(a). We connect our Linux-based laptop to the E312 via a serial USB cable. Then, we generate a continuous wave (CW) and measure the RMS power via a Rohde & Schwarz spectrum analyzer that was connected to the output port of the E312. The same cables, which had a measured loss of 0.4 dB, were used in our in-field experiments. Calibration results are given in Table I.

V. User-Free Ground-to-Ground and UAV-to-Ground Channels

In this section, we briefly discuss our measurement results for the user-free GtG and AtG channels. A user-free AtG experiment

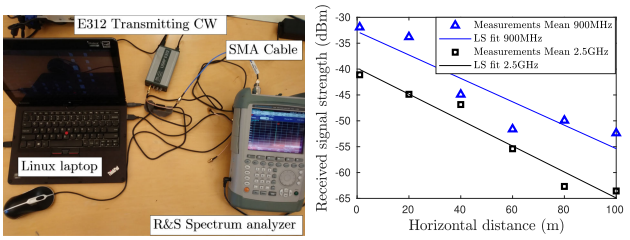

(a) (b)

Fig. 3. (a) Power calibration setup for USRP E312. (b) User-free measurement results for the Ground-to-Ground setup at 900 MHz and 2.5 GHz.

TABLE I
MEASURED TRANSMIT POWER (dBm) IN USRP E312

Gain (dB)	40	45	50	55	60	65	70
f_c=2.5 GHz	-14.2	-18.8	-13.6	-8.7	-3.8	1.2	6.2
f_c=900 MHz	-24.3	-19.7	-14.4	-9.2	-4.3	-0.3	0.4

is shown in Fig. 2(d) (left). The objective of these two experiment setups is two-fold: (*i*) to create a baseline understanding of the conventional ground-based channel and see how it might differ from a UAV-based link, and (*ii*) to investigate the UAV-to-Ground channel with no user/human body involvement to directly compare to when a user is holding the UE.

A. User-Free GtG Measurements Results

In this set of experiments, both the Tx and Rx are mounted on tripods about 1.5 m above the ground. With no human near or holding the receiving USRP, the received signal is averaged over 15 seconds per Rx location. The average RSS levels with their first-order, least-squares fit are plotted in Fig. 3(b) for both carrier frequencies.

We see that the results follow the expected behavior of terrestrial networks, where the received signal is reduced by increasing the separation distance. This reduction can be described by the log-distance pathloss model. In particular, $PL(d) = PL(d_{ref}) + 10n \log \frac{d}{d_{ref}} + \chi_{\sigma_s}$, where $PL(d)$ is the pathloss at a distance d, χ_{σ_s} is the shadowing parameter, $PL(d_{ref})$ is the pathloss at a reference distance, and n is the pathloss exponent. If we take $d_{ref} = 20$m as our reference distance measurement, a value of $n = 2.53$ can be obtained, which is quite common for LOS experiments in this environment [26]. Moreover, the standard deviation of the shadowing parameter, σ_s, is estimated as 3.2 dB.

B. User-Free UAV-to-Ground Measurement Results

Let us now examine the AtG channel with the same Rx still mounted on the tripod but with the Tx being mounted on the UAV (see Fig. 2(a)). As explained in Section III, the Tx UAV visits six locations per altitude while the ground Rx records the received signal.

Average RSS: The mean values of the obtained RSS levels at 900 MHz and 2.5 GHz are shown in Fig. 5 as dashed lines. On the whole, we can see the distinction between the AtG and GtG channels. The AtG channel results follow a curve instead

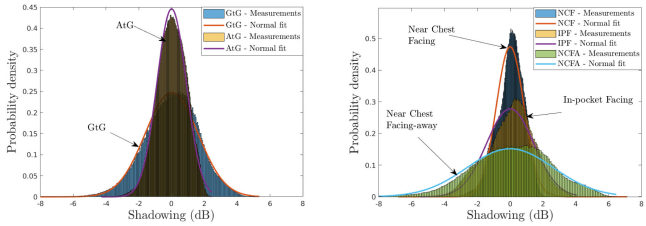

(a) (b)

Fig. 4. Shadowing at 900 MHz for the (a) user-free GtG and AtG experiments, and (b) the three use cases in AtG channels.

of the expected straight line obtained by the GtG experiments. This curved behavior is explained here. At $d = 0$ m (*i.e.*, when the Tx UAV is directly above the Rx), low RSS levels are experienced. These results are due to two factors: the antenna elevation radiation pattern (Fig. 2(c)) and the UAV body. Since the Tx and Rx antennas are vertically-mounted, omni-directional antennas, the radiated power is at the minimum value in the vertical direction (*i.e.*, $\theta = \arctan(\frac{h}{d}) = 90°$). As a result, we expect to see lower RSS levels at this location compared to other distances/altitudes with angles less than 90°. Furthermore, due to the antenna being mounted on the UAV body, the transmitted signal is partly blocked by the UAV body, especially when seen from a below node. As the Tx UAV moves to the next locations, the Rx starts to experience a stronger received signal due to greater alignment of the radiation pattern and less drone body obstruction. The mean RSS reaches its maximum value between 20 and 40 m horizontal distance for all altitudes. Then, mainly due to its inverse relationship to distance, the received power starts to decrease in a way that is similar to the conventional terrestrial links. It is interesting to see that for a fixed UAV altitude, the RSS can vary by as much as 20 dB as the UAV moves from one location (above the ground Rx) to another, only 20 m away from the ground Rx. This significant change in RSS is attributed to the elevation radiation pattern of the antennas.

Shadowing: Shadowing in this work is caused by either the drone body [29] or the user's body or a combination of both. In other words, other forms of obstructions are not experienced in this study. As either body becomes an obstacle in the signal path, shadowing will occur and it will be a function of how much of the obstacle is obstructing the receiver path. We calculate shadowing by subtracting the received power from its average value [31] and analyze its distribution. First, we report that the measured shadowing (also true for all other use cases) can be modeled as a zero mean Gaussian random variable with its standard deviation (in dB) depending on the investigated scenario. Second, we find that the user-free UAV-to-ground channel, except for the directly-above hovering position, results in less shadowing compared to the user-free ground-to-ground channel. We can see an example of this effect in Fig. 4(a), where we plot the shadowing at 900 MHz and location (d_3, h_1). Third, to directly compare shadowing of the user-free scenario to the results involving the user, let us compare Fig. 4(a) to Fig. 4(b). We can see that user orientation can significantly alter the standard deviation of the shadowing parameter. This result is evident by the exhibited larger spread in the Near Chest Facing-away compared to the

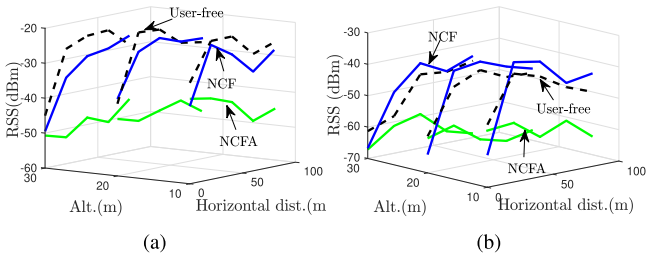

Fig. 5. Average RSS levels for the user-free, NCF, and NCFA scenarios for all UAV hovering positions at (a) 900 MHz and (b) 2.5 GHz.

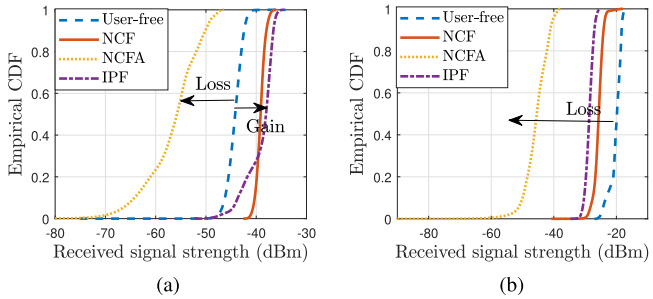

Fig. 6. RSS CDF for the three use cases and the user-free scenario at (a) 2.5 GHz and (b) 900 MHz for UAV hovering position (d_2, h_2).

other two use cases at which the user is facing the UAV. We will elaborate on the shadowing standard deviation for all use cases in the next section.

VI. Average Gain/Loss, Shadowing and Multipath Effects in UAV-to-User Channels

In this section, we investigate how different use cases of holding a UE can affect: (*i*) average RSS levels, (*ii*) shadowing, (*iii*) multipath characteristics, and (*iv*) the Rician K-factor of an AtG channel at various drone altitudes, locations, and carrier frequencies. In doing so, we consider the relative impact of user-versus-UAV properties on the resulting wireless channel characteristics at ultra-low drone altitudes.

A. Average RSS and User-Induced Loss/Gain

Here, we define user-induced loss/gain as the difference in RSS between the baseline (User-free) scenario and the facing and facing-away scenarios when the user holds the UE close to the chest. Fig. 5 shows the average RSS for these three scenarios (user-free, NCF, and NCFA) at both frequencies.

User-Induced Gain Compared to Free Space. To investigate how the existence of the human body can affect the UAV-to-ground channel, we first compare the results of the Near Chest Facing (NCF) scenario to those obtained in the user-free experiment. Visually, this comparison could be made by inspecting Fig. 5. We find that the body of the user when facing the transmitting UAV can actually result in *increased* RSS levels. For example, while the mean RSS level at (d_5, h_1) is -46.2 dBm in the user-free setup, it is -40.3 dBm when the user holds the UE facing the transmit UAV (*i.e.,* NCF), a 5.8 dB increase in the mean RSS. At the location of (d_2, h_3), a 7.6 dB increase in the mean RSS level is experienced due to the existence of the user body. Similar results are found when the UE is inside the user's pocket. We have previously observed this effect in a GtG channel [8], where the user's body was found to result in a 14% increase in throughput over a reference, user-free setup. However, it is worth noting here that the above finding depends on the UAV hovering position. For example, at 0 m horizontal distance (*i.e.*, when the UAV is directly above the user), the existence of the user's body and orientation becomes almost irrelevant to the average RSS changes, as the gain/loss compared to the baseline are minimal (less than a standard deviation). Other works have also shown that the human body can increase the radiation of the antennas, such as [8], [10], [15]. We conclude that, compared to a user-free scenario, there exists a user-induced *gain* that yields increases in RSS levels when the UE is facing a transmitting, in-flight drone when a free-space path exists from sender to receiver. This *gain* can reach an average and a maximum value (across all locations at 2.5 GHz) of 3.4 dB and 12.05 dB, respectively, and is a function of the UAV hovering position. Finally, we report that with the exception of three hovering positions, average user-induced gains compared to free space at 900 MHz were insignificant, *i.e.*, less than the standard deviation of the measured signal. This might be due to the fact that the human body absorbs more power at low frequencies compared to higher frequencies at which it can reflect more power [19]. A similar effect is shown in [21] where three different human bodies were studied at 17 different frequencies. It was concluded that the radiated and attenuated power (P_{rad} and P_{loss}) across frequencies can vary according to the human body type and that gains with respect to free-space were achieved at higher frequencies, while at low frequencies, absorption resulted in no recorded gains.

User-Induced Loss Compared to Free Space. Next, we seek to understand the role of the human body on the channel when the user's orientation changes (*i.e.*, the whole body is in the path of the signal). To do so, we compare the measured RSS samples in the Near Chest Facing-away (NCFA) scenario to those obtained in the baseline (User-free) setup. We find that the user's body indeed causes reductions in the average RSS, which is clear via visual inspection of Fig. 5. In particular, if we exclude the strictly-vertical UAV position at which the user's orientation is virtually irrelevant, the user's body is found to considerably reduce the average RSS. At 2.5 GHz, an average reduction of 13.2 dB and a maximum reduction of 23.1 dB across all drone hovering positions is experienced. An example of this loss at 2.5 GHz for location (d_2, h_2) is shown in Fig. 6(a) with an average value of 12.3 dB. Higher loss is measured at 900 MHz, with an average and maximum reduction of 17.5 dB and 26.3 dB, respectively. An example of this loss at 900 MHz is shown in Fig. 6(b). This result is in line with the finding above, as the body of the human subject involved in this study is found to result in more attenuation (most likely through absorption) at this frequency than 2.5 GHz. Similar values of human-induced losses compared to free-space can be found in literature [9].

Impact of User Orientation. Now that we understand how the user's body can affect the channel compared to a free-space

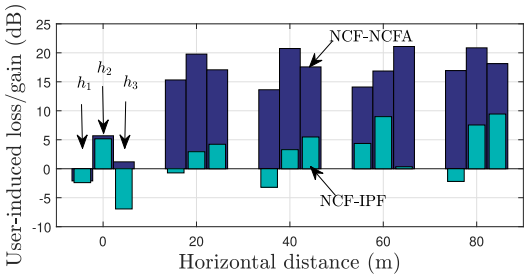

Fig. 7. Impact of body blockage (blue bars) and change in UE near body location (grey bars) on received signal strength at 900 MHz.

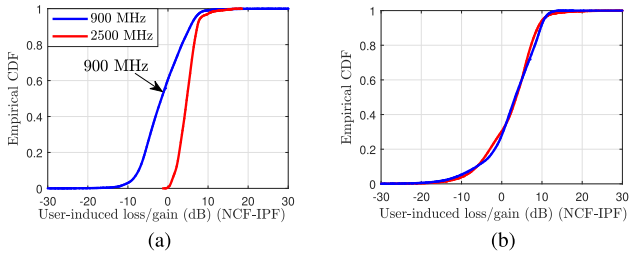

Fig. 8. Impact of placing the UE inside pocket at two frequencies at drone altitudes (a) $h_1 = 10$ m and (b) $h_3 = 30$ m.

baseline, it is interesting to compare for the same person how their orientation and near-body location of the UE can affect the UAV-to-ground channel. First, we compare the NCFA measurements to those obtained in the NCF (Near Chest Facing) scenario. This corresponds to calculating the difference between the two cases, *i.e.,* $NCF - NCFA$. The results of this difference at 900 MHz are plotted (in blue bars) in Fig. 7. We can see that the human body results in signal blockage significantly reducing the average RSS. These losses can reach a maximum of 21 dB at 900 MHz (and 25 dB at 2.5 GHz). Interestingly, this observation does not apply to the strictly-vertical location, as the user's orientation is arbitrary relative to the UAV and the difference between the two cases is minimal. The effect of this UAV hovering position can be clearly seen in Fig. 7, where the first horizontal distance ($d = 0$ m) has both negative and positive average values of the investigated impact. As we move to the next hovering positions, however, the human body blockage starts to be quite consistent, ranging between 15 dB and 21 dB across all locations. Similar reductions due to user blockage can be found in [9], [15], [23].

Impact of Near-Body Location for a Fixed User Orientation. For the same drone hovering position and the same user orientation of facing the transmit UAV, we investigate if placing the UE near different body locations yield different received signal strengths. To do so, we calculate the difference in average RSS level in NCF and IPF scenarios (*i.e.,* $NCF - IPF$) and analyze the results. This difference at 900 MHz is plotted (in grey bars) in Fig. 7. First, we see that placing the UE inside the pocket causes reductions in average RSS levels, which is evident by the positive loss across many hovering positions. This degradation can reach around 8.5 dB. Interestingly, we find that this difference is not constant and can change by altering the drone's hovering altitude. Specifically, the difference increases as the UAV's hovering altitude increases. This trend can be seen in Fig. 7. For example, at 40 m distance and 10 m altitude, the average difference between the two use cases is around -2.5 dB. At a 30 m altitude of the same horizontal distance, this difference is about +5 dB (a 7.5 dB increase in difference). This improvement (negative dB values at low altitudes) could be attributed to the fact that, as the drone hovers at lower altitudes, it starts to exhibit a stronger LOS with the UE inside the pocket, and as a result, the difference between the two use cases decreases. This finding is consistent across all but the first hovering position. We also find that this behavior (stronger RSS in IPF compared to NCF at h_1) occurs mostly at 900 MHz but not at 2.5 GHz, and it diminishes as we go to higher altitudes. Fig. 8 shows the difference in RSS due to placing the UE inside the pocket at two frequencies, averaged over all distances for h_1 and h_3. From Fig. 8(a), we can see that, at h_1 with the 900 MHz carrier frequency, about 60% of NCF-IPF values are negative, indicating stronger IPF while no such values are recorded at the same altitude for 2.5 GHz. As we move to higher altitudes, the distinction between two frequencies become negligible with an almost identical CDF at h_3 (see Fig. 8(b)) and the same trend of stronger NCF signal levels. This effect might be attributed to the longer wavelength at 900 MHz (33 cm) and better penetration characteristics compared to 2.5 GHz (12 cm). However, more investigation is needed.

Recalling that the user's orientation is fixed (facing the UAV), *we conclude that there exists not only an optimal UAV position for a UAV-to-user connectivity based on their orientation, but there also exists an optimal UE location on/near their body when facing the UAV in a LOS setup.* This result could influence drone placement algorithms that seek to dynamically adapt to different user gestures based on wireless sensor measurements.

It might be worth mentioning that if the experiments were to be conducted in an indoor environment, we expect that due to reflections and contributions from the surrounding walls/ceiling, the human body will have less of an impact on the channel. This speculation comes from the findings of many indoor studies that investigated the human body impact on wireless channels such as [9], [56].

B. Shadowing and Multipath Due to UAV and User Bodies

In this section, we discuss how shadowing and multipath are affected by the UAV, its mounted antenna radiation pattern, and the human body. Specifically, we investigate how these factors can impact the shadowing standard deviation and the multipath parameter (σ in (5)). Fig. 9(a) shows the instantaneous RSS when the UAV is directly above the user (*i.e.*, at (d_1, h_1)). Conversely, Fig. 9(b) illustrates the RSS when the UAV is at d_2 at the same altitude (*i.e.*, at (d_2, h_1)). Fig. 9(c) shows the estimated multipath parameter, from measurements and the fitted Rician model at one altitude of 20 m across all distances. There are two important observations to be made here.

Impact of the elevation radiation pattern and UAV body on shadowing standard deviation. Even though the separation distance increases from when the drone is hovering above the user (d_1, h_1) to when the UAV is at (d_2, h_1), (*i.e.,* from

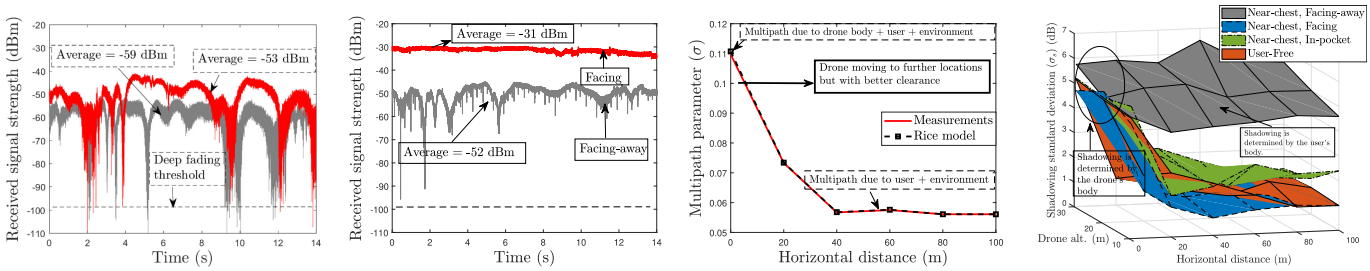

Fig. 9. Effect of UAV body on shadowing and multipath effects. (a) Drone is hovering directly above the user at $d_1 = 0$ m, $h_1 = 10$ m; significant multipath resulting in multiple deep fading events. (b) Drone is 20 m away resulting in less multipath effects and a more stable signal level with no deep fading events. Also, a significant increase in signal level is experienced due to better radiation pattern product and less shadowing caused by the drone body. (c) The Rician multipath parameter σ obtained from measurements and Rician fit versus drone hovering distances at h_2; it is noticeable that as the UAV moves away from the strictly above location less multipath is exhibited by the ground user. (d) Shadowing standard deviation across all locations at 2.5 GHz.

$d_x = \sqrt{d_1^2 + h_1^2} = \sqrt{0^2 + 10^2} = 10$ m to $d_x = \sqrt{d_2^2 + h_1^2} = \sqrt{20^2 + 10^2} = 22.36$m), which would lead us to expect a reduction in the received power by an approximate 7 dB as a result of the inverse relationship between received power and distance, the received power actually increases by 28 dB in the facing scenario.

The increased received power can be explained by the increased power in the radiation pattern of the antennas along the elevation plane and the reduced UAV body shadowing. The elevation radiation pattern of the omni-directional dipole antenna, which is depicted in Fig. 2(c), clearly shows that at strictly-vertical links ($\theta = +/-90$) the antenna experiences significant reductions in its radiated power. This is in line with the theory that indicates zero radiated power in the vertical plane (*i.e.,* $G_{Tx}(\theta) = \cos(\theta) = \cos(90) = 0$) [49], [50]. In addition to this, the UAV body acts as an obstruction, causing shadowing (reduction in the strength of the otherwise LOS component) and an increase in multipath effects. As the UAV moves from d_1 to d_2, there becomes more clearance in the Tx-Rx path and less obstruction/shadowing caused by the drone body, and the radiation pattern product $G_{Tx}G_{Rx}$ becomes stronger. For example, the radiation pattern product at 20 m horizontal distance and 10 m altitude is $G_{Tx}G_{Rx} = \cos^2(\theta) = \cos^2(\arctan(\frac{10}{20})) = 0.8$. This value corresponds to -0.97 dB which, compared to approximately -35 dB (assuming a $\theta = 89°$), is a significant increase in received power value. This reasoning holds for the facing scenario, regardless of the UE near-body location. When the user is facing-away, as the UAV moves to d_2, the increase in the RSS level, which was previously obtained due to the radiation pattern impact, is now negated by the impact of the user's body. That is, even though the UAV moves to a location where the elevation radiation pattern is much stronger and with a less obstructed path by the UAV body, the user's body now becomes the main obstruction, and the received signal ultimately remains approximately the same as when the drone hovers above the user (see Fig. 9(b)).

We have investigated the shadowing standard deviation for all experiments and found that it is greatest when the UAV is directly above the user (at d_1) with values of $\sigma_s > 4$ dB (reaching up to 6 dB) across all experiments and frequencies. Then, it gradually decreases as the UAV moves to more-distant locations that have a less obstructed Tx-Rx path. This behavior occurs in both scenarios of facing and in-pocket, and it can be clearly seen in Fig. 9(d), where we plot σ_s (shadowing standard deviation) for all UAV locations at 2.5 GHz.

A similar result (with a slightly less σ_s) is found at 900 MHz and summarized in Table II. *We then conclude that in LOS UAV-to-User channels there exists two regions for shadowing: one that is dependent on the UAV body and another that is mainly affected by the user's body*. This conclusion excludes any external/environmental causes. That is, the observed effects are due to either the UAV or the user, not any environmental changes.

Impact of the UAV body on multipath. When the UAV is flying directly above the user, the multipath experienced at the receiver is stronger than in any other UAV hovering location. This result holds true across all frequencies and use cases. We can clearly see this effect by comparing two figures in Fig. 9. Let us define a deep fading event to be that at which the SNR falls to approximately 0 dB. At this value, the packet delivery ratio of many off-the-shelf IEEE 802.11 products could fall between 0% to 5% [44], [45], indicating the potential of a complete loss of data packets. Our measured noise floor is in the range of -100 dBm to -105 dBm. If we observe Fig. 9(b), which corresponds to location (d_2, h_1), we see that the received signal is characterized by no deep fading events and the fading events that occur still give us an SNR of at least 10 dB. However, when the UAV is hovering directly above the user (Fig. 9(a)), this is not the case: multiple deep fading events occur, where the received signal falls to extremely low levels, indicating strong destructive interference effects. More specifically, during a time duration of 15 seconds, more than 10 deep fading events can occur as a result of the UAV body being strictly above the user. To understand how multipath is induced by the UAV body and how it can dramatically change depending on the drone's relative UAV location and consequently the Tx-Rx path clearance, let us examine Fig. 9(c). In this figure, we plot the estimated multipath parameter (σ in equation (5)) across all distances for a fixed UAV altitude. Both the value obtained from measurements and that from fitting a Rician distribution are plotted. When the UAV is directly above the user, we obtain $\sigma = 0.11$. As the UAV transitions to the next location, it falls to 0.075 and then settles

TABLE II
SHADOWING STANDARD DEVIATION AT 900 MHZ

Drone loc.	Near-Chest Facing (NCF)						In-pocket Facing (IPF)						Near-Chest Facing-Away (NCFA)					
Dist. / Alt.	d_1	d_2	d_3	d_4	d_5	d_6	d_1	d_2	d_3	d_4	d_5	d_6	d_1	d_2	d_3	d_4	d_5	d_6
h_1 (10 m)	4.76	2.40	2.13	1.53	1.97	1.08	4.05	2.47	3.33	1.9	3.61	2.4	4.96	3.26	3.18	3.78	3.79	4.6
h_2 (20 m)	4.16	2.67	2.46	2.36	0.89	0.82	4.04	1.97	1.12	1.35	1.27	1.45	5.09	3.74	4.56	3.52	5.76	5.09
h_3 (30 m)	4.98	2.6	2.04	1.42	0.84	0.99	3.19	2.13	2.22	1.43	1.22	1.18	4.66	5.39	5.15	3.60	3.62	5.53

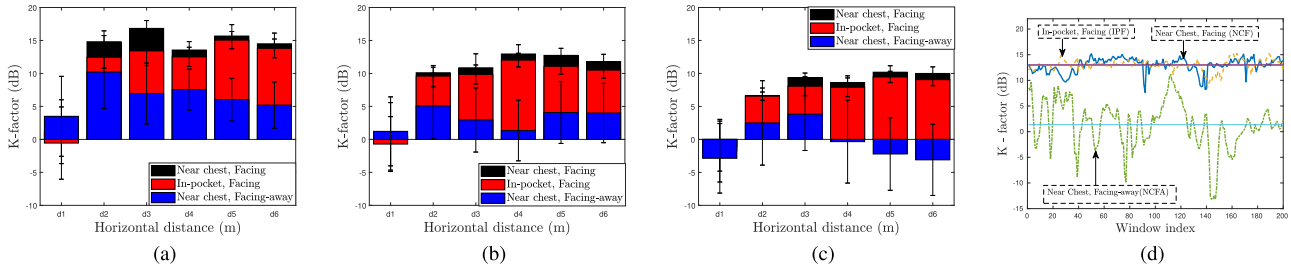

Fig. 10. The average and standard deviation of the measured Rician K-factor for the three use cases of the LOS UAV-to-Ground channel at 2.5 GHz and a UAV altitude of (a) 10 m, (b) 20 m, and (c) 30 m. (d) The time-varying nature of the K-factor as a function of the use case.

at around 0.055, which is a 50% decrease in multipath from when the UAV is strictly above the user. It is interesting to note that a similar curve was obtained by [37] with a model that describes how multipath decreased with increasing drone height. However, here, the altitude is fixed, and the only variable is horizontal distance, which corresponds to the Tx-Rx path clearance.

VII. THE RICIAN K-FACTOR IN UAV-TO-GROUND CHANNELS FOR DIFFERENT USE CASES

In this section, we present how the Rician K-factor, which is a measure of channel fading severity, can be influenced by the user's orientation, UE near-body location, and the UAV's hovering location. Before elaborating on these scenarios, the time-varying nature of the K-factor as a result of the UAV's continuous hovering is addressed.

A. Impact of UAV Hovering and User Body on the K-Factor's Time Variability

The UAV's continuous movement while hovering could result in variations in the K-factor. That is, the main LOS component and/or the multipath components from one window to another, might vary. To visualize the issue, Fig. 10(d) shows the calculated K-factor for 200 windows (approx. 13 seconds of hovering duration) at location (d_4, h_2). We first consider the case where the user is facing the drone (NCF or IPF). We see that the K-factor varies within a range of 4 dB (10 dB to 14 dB). The average value for both cases, however, is approximately the same. This variation in the K-factor is due to the time-varying nature of the channel, which is a result of the UAV's hovering motion that causes $\alpha_n(t)$ and $\Phi_n(t)$ in (1) to change. Recall that the user is fixed, and there is no moving objects in the experiment's environment. When the user's body is added to the equation (*i.e.*, the user is facing-away), severe fluctuations are experienced in the K-factor, and the mean value becomes unstable. This is clear in the NCFA plot in the same figure, where the value of K can vary from -12 dB to 10 dB (22 dB range). After investigating the K-factor variance as a function of the user's body, we found that a worst case scenario of 20-times stronger variance is observed as a result of fluctuations induced by the user's body. These strong fluctuations could be attributed to the random nature of multipath reflections caused by propagation through the human body [22]. The time-varying nature of the K-factor has been addressed in [30], but the experiments were conducted with a high-altitude platform in an urban area; in other words, variations in the K-factor where not specifically due to a UAV's hovering state nor the user's body, but variations in the urban environment. Similarly, the work in [31] characterized the K-factor for low-altitude UAVs, but the experiments were done in an urban environment crowded with buildings and spanned large horizontal distances. The work in [22] leveraged the time-varying nature of multipath reflections within the body to achieve beamforming using signals of different frequencies.

B. Rician K-Factor When Facing Tx UAV

In this section, we analyze the Rician K-factor when the user is facing the Tx UAV. The average value and standard deviation of the Rician K-factor at 2.5 GHz for all use cases across all locations is plotted in Fig. 10.

First, we see that, for a fixed altitude, the Rician K-factor experiences a significant change as the UAV moves from d_1 to any other hovering position. For example, in Fig. 10(a), when in-pocket and at a UAV altitude of 10 m, the average K-factor can change from approximately $\overline{K} = 0$ dB when the UAV is above the user (*i.e.*, $d_1 = 0$ m) to $\overline{K} = 12$ dB as the UAV hovers at $d_2 = 20$ m. Such a dramatic change in the K-factor is attributed to the impact of both the elevation radiation pattern of the vertically-oriented antenna and the body of the UAV. Recall that a vertically-oriented omni-directional dipole antenna theoretically does not radiate in the vertical direction.

TABLE III
AVERAGE K-FACTOR AT 10 M DRONE ALTITUDE FOR 900 MHZ AND 2.5 GHZ IN THE THREE USE CASES

Frequency	NCF	IPF	NCFA
900 MHz	20.65	17.92	13.41
2.5 GHz	12.6	11.2	6.63

In reality, however, there will still be some radiated power at significantly-less levels. This radiation-pattern effect will impact the main LOS component of the received signal, while the body of the UAV and its induced reflections will cause a larger value of the multipath component (σ in (5)). The net result of this effect is the significant reduction in the K-factor, which we observed at d_1, at all altitudes and both frequencies.

The K-factor also, for the same horizontal distance, decreases when increasing the drone altitude. For example, if we examine the results of the K-factor at d_2 for the near-chest scenario, we see that it decreases from around $K = 15$dB at $h_1 = 10$m to $K = 10$dB at $h_2 = 20$m to approximately $K = 7$dB at $h_3 = 30$m. This reduction in value is mainly due to increases in distance and the radiation pattern misalignment loss, both of which will cause reductions in the strength of the main LOS component.

C. Rician K-Factor When Facing-Away From Tx UAV

If the user is facing-away from the transmitting UAV, the question becomes how severe the user's impact is on the channel and the Rician K-factor and whether or not it turns into a Rayleigh channel ($K = -\infty$ dB).

We find that in all but one location, where the Tx UAV hovers directly above the ground user, the K-factor experiences great reductions as the user faces-away from the flying UAV. This is clear in the results plotted in Fig. 10. At h_1, for example, the difference in K-factor between facing and facing-away for the same body position (near chest) can reach up to 11 dB and an average value across all locations of 6.18 dB. As the UAV moves to higher altitudes and the general trend of the K-factor tends to result in weaker values for all scenarios, the user's body blockage starts to result in negative values (in dB) at h_3, suggesting an extremely weak LOS component and an increase in multipath effects.

D. Frequency Impact on K-Factor

To investigate how carrier frequency can affect channel fading severity measured by the K-factor, we compared the average values of the K-factor at both frequencies across all three use cases. We found that across most measurements, the K-factor at 900 Mhz was higher than in the 2.5 GHz results. Comparison results at h_1 are given in Table III. The stronger K-factor at 900 MHz is evident across all three use cases, reaching an average and maximum difference of 7.18 dB and 11.3 dB, respectively. However, slightly larger variance in the K-factor is observed at 900 MHz. Similar findings (higher K-factor values and a larger dynamic range at 900 MHz with the presence of humans) are reported in [51]. Due to stronger K-factor values at 900 MHz, the values obtained when facing-away are positive in dB, indicating a stronger ratio of LOS to scattered/multipath

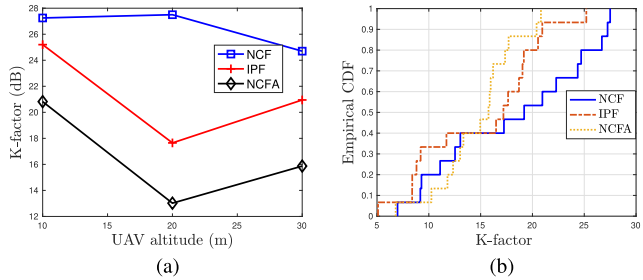

Fig. 11. (a) Average K-factor for the three use cases at one horizontal distance and different UAV altitudes at 900 MHz. (b) The empirical CDF of the average K-factor across all locations and use cases at 900 MHz.

power than that at 2.5 GHz. An example of the 900 MHz K-factor is given in Fig. 11. To the left (Fig. 11(a)) the average value at d_5 for the three cases is shown. If we compare those to the values obtained at the same location but at 2.5 GHz (Fig. 10(b)), we can see that the NCFA K-factor at 900 MHz is about 8 dB stronger. To further investigate this frequency dependence, we compare all average values of the K-factor at 900 MHz (Fig. 11(b)) to those obtained at 2.5 GHz (Fig. 10). We can first notice that, while there exists no negative dB values of the K-factor at 900 MHz, at 2.5 GHz and a UAV altitude of 30 m, many instances result in negative K-factor values. Moreover, we can see that about 50% of the values at 900 MHz exceeds 17 dB for NCF and IPF, while no values reach that level at 2.5 GHz.

The above discussion reveals that using lower frequencies might result in a more deterministic behavior of UAV-based fading channels. This finding might be attributed to the fact that lower frequencies have a longer wavelength and therefore are less sensitive to UAV hovering jitter/fluctuations error. Designers of UAV-based AtG channels should expect about 7 dB degradation in K-factor values as they move from 900 MHz to somewhere near 2.5 GHz, and protocols, in terms of adaptive power control and required SNR – to meet certain bit error rates – should change accordingly.

E. Is Rician Distribution a Good Fit for All Three Cases?

While it might be expected that the channel follows a Rician distribution in NCF and IPF scenarios, it is interesting to see if this assumption still holds when facing-away from the UAV. Therefore, to test the assumption of the Rician channel for all three scenarios at both frequencies, we fit a Rician distribution using the Maximum Likelihood Estimate (MLE) to the measured values of the normalized received signal envelope for various time durations and compare the obtained fit to the measurements.[2] The comparison shows that the Rician model can adequately represent the channel for all three scenarios with an average RMSE error of 4.99E-03 and 4.16E-04 in a and σ (of equation (5)), respectively. This result indicates that, even though the main LOS component was shadowed by the human body in the NCFA case, there still exists a dominant component

[2]This was also done for a similar experiment setup at the same location in our previous work [29].

TABLE IV
PARAMETERS OF THE LOS UAV-TO-USER CHANNEL IN NCF SETUP

	Measured		Rician Fit		Error	
dist.	a	σ	a	σ	$RMSE_a$	$RMSE_\sigma$
d_1	0.643	0.1097	0.633	0.1107	0.01	9.41E-04
d_2	0.7877	0.0733	0.7843	0.0734	0.0035	1.61E-04
d_3	0.8462	0.0567	0.8443	0.0568	0.0019	6.38E-05
d_4	0.8552	0.0575	0.8533	0.0561	0.0019	6.07E-05
d_5	0.8029	0.0561	0.8008	0.0576	0.0021	4.57E-05
d_6	0.798	0.063	0.7958	0.0631	0.0025	9.77E-05

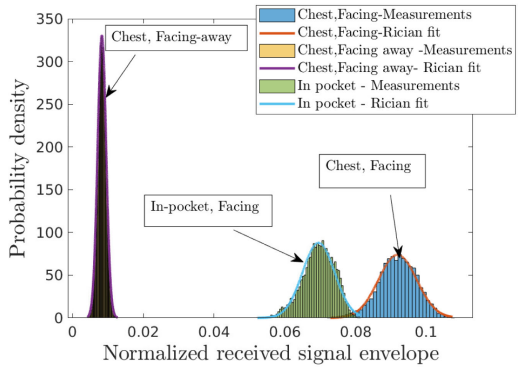

Fig. 12. Histogram of the measured values of the normalized received signal envelope and its fitted Rician distribution at a drone altitude of 20 m.

compared to the multipath/scattered component captured within that time period. A summary of the obtained parameter values through measurements and the Rician fit for a UAV altitude of $h_2 = 20$ m in the NCF scenario are given in Table IV. We see that the Rician model is a good fit for all UAV positions, even d_1 (drone directly above user). An example of the measured normalized received signal envelope and its Rician fit when the UAV is 80 away at h_2 is shown in Fig. 12. We see a close proximity between the histogram of measured data and the Rician fit. In addition, the impact of the user's body on the measurements is clear; the measurements are distributed, from lowest to highest, in the following order: near chest facing-away (NCFA), in-pocket facing (IPF), and near-chest facing (NCF). We note that, even though the signal path is obstructed by the user's body, the received signal envelope still follows a Rician distribution in the facing-away scenario, indicating that there still exists a dominant signal component, however, at a significantly lower level compared to the other two scenarios.

VIII. APPLICATIONS: HUMAN-BASED DEPLOYMENT OF UAVS FOR OPTIMAL SECRECY

The obtained insight from this work can find various applications. The focus here is on physical layer security and secrecy maximization based on the orientation of ground users relative to ultra-low UAVs.

Physical layer security has been recently proposed for UAV-based communication systems [53]–[55]. However, none of these works consider the human-body effect, its orientation, and the UAV-body impact on wireless channels to understand real-world physical layer security performance. Here, based on the collected experimental measurements of UAV-to-user channel for different UAV positions and human body orientations, we show that the average secrecy performance of UAV-based wireless communication systems for different low-altitude UAV positions and human body orientation is significantly different compared to the theoretical analysis on physical layer secrecy performance that do not consider user and drone body effects [53]–[55].

TABLE V
SECRECY PERFORMANCE OF UAV 1'S SIGNAL AT DIFFERENT LOCATIONS OF UAV 1 WHEN UE 1 FACES EAST AND UE 2 FACES WEST

Alt. \ Dist.	0 m	20 m	40 m	60 m	80 m	100 m	120
10 m	0	0	0	0	8.75	3.12	5.61
20 m	0	0	0	0	8.72	5.13	6.37
30 m	0	0	0	0	7.88	4.70	5.04

Consider a UAV-assisted wireless communication system with two UAVs and two users as shown in Fig. 13. The location (0,0) is shown with a 'red dot' in Figs. 13(a) and (b), and users 1 and 2 are located at (0, 40) m and (0, 80) m, *i.e.*, 40 m apart from each other. Each UAV can move to one of the locations $(i \times 10, j \times 20)$ m where $i \in \{1, 2, 3\}, j \in \{0, .., 6\}$, as marked with 'blue dot's in Figs. 13(a) and (b). The UAVs 1 and 2 aim to send confidential messages to users 1 and 2, respectively, and interference can be avoided by using two separate carrier frequencies, 2.5 GHz and 900 MHz for signals intended for users 1 and 2, respectively. Each user i tries to overhear the signal intended for the other user j which is transmitted from UAV j ($i, j \in \{1, 2\}, j \neq i$). We investigate the secrecy performance for such a network with two different user orientation configurations; (1) User 1 is facing east while user 2 is facing west, as shown in Fig. 13(a), and (2) Both users are facing west, as shown in Fig. 13(b). We measure secrecy performance for each user for a given configuration in terms of ergodic secrecy rate. For a given location l of UAV i, the instantaneous secrecy rate for user i at time slot n can be defined according to [52]:

$$r^l(n) = \left[\log_2\left(1 + \gamma_i^l(n)\right) - \log_2\left(1 + \gamma_j^l(n)\right)\right]^+ \quad (6)$$

Here, $\gamma_i^l(n)$ and $\gamma_j^l(n)$ are the SNR for UAV i to user i and UAV i to user j at time n ($i, j \in \{1, 2\}, j \neq i$), respectively, and $[x]^+ = \max(x, 0)$. Then, the ergodic secrecy rate can be obtained as follows:

$$\mathcal{R}^l = \frac{1}{N}\sum_{n=1}^{N} r^l(n) \quad (7)$$

Here, N is the total duration of measurements in terms of number of time slots. The ergodic secrecy rate for UAV 1's signal for different UAV 1's locations in case of configurations 1 and 2 are shown in Tables V and VII, respectively and the ergodic secrecy rate for UAV 2's signal for different UAV 2's locations in case of configurations 1 and 2 are shown in Tables VI and VIII, respectively.[3] It can be observed that the ergodic secrecy rate for

[3]We assume that RSS measurements for each UAV-to-user channel can be obtained at the UAV since both users are part of the communication system. Therefore, the UAVs can determine users' orientations and locations using

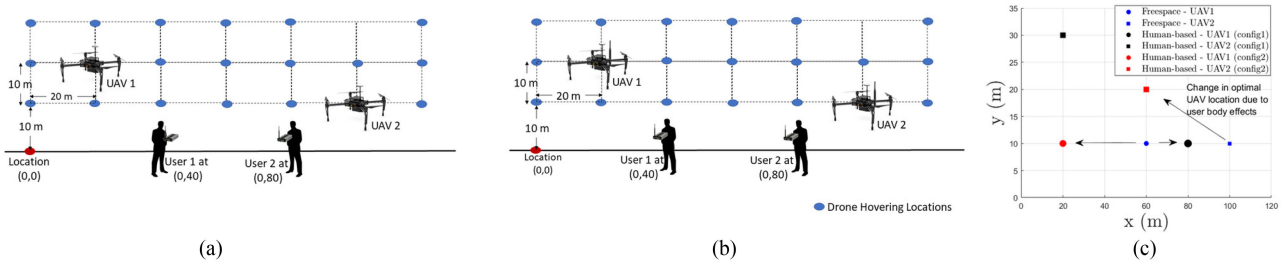

(a) (b) (c)

Fig. 13. Illustration of human-based physical layer security for UAV-assisted networks. (a) User 1 faces east and User 2 faces west, (b) Both Users face west. (c) Impact of including the human-induced effects on optimal location of UAVs for maximum secrecy, where marker size is proportional to secrecy rate.

TABLE VI
SECRECY PERFORMANCE OF UAV 2'S SIGNAL AT DIFFERENT LOCATIONS OF UAV 2 WHEN UE 1 FACES EAST AND UE 2 FACES WEST

Alt. \ Dist.	0 m	20 m	40 m	60 m	80 m	100 m	120
10 m	4.14	1.72	4.10	0	0	0	0
20 m	6.04	6.76	4.98	0	0	0	0
30 m	6.97	7.63	6.33	0	0	0	0

TABLE VII
SECRECY PERFORMANCE OF UAV 1'S SIGNAL AT DIFFERENT LOCATIONS OF UAV 1 WHEN BOTH UES FACE WEST

Alt. \ Dist.	0 m	20 m	40 m	60 m	80 m	100 m	120
10 m	2.34	3.30	0	0	1.25	0.29	0.41
20 m	1.85	0.68	0	0	1.14	0.17	0.92
30 m	0.41	0.17	0	0	2.73	0.63	0.16

TABLE VIII
SECRECY PERFORMANCE OF UAV 2'S SIGNAL AT DIFFERENT LOCATIONS OF UAV 2 WHEN BOTH UES FACE WEST

Alt. \ Dist.	0 m	20 m	40 m	60 m	80 m	100 m	120
10 m	0.16	0	4.10	5.08	0.91	2.98	1.54
20 m	0.09	0.46	4.98	6.60	2.12	0.20	1.23
30 m	1.13	1.96	6.33	5.67	0.68	0.46	0.33

a given user i is impacted by UAV i to users i and j distances as well as the factors that determine the shadowing effect on these channels, *e.g.*, carrier frequency and the orientation of each user. As shown in Tables V–VIII, the ergodic secrecy rate of user i is low when UAV i is behind or above the user i while user j is facing UAV i, and the ergodic secrecy rate of user i is high when user i is facing UAV i while the UAV is behind the user j. The reason is that the shadowing effect on a UAV-to-user channel is less when the user is facing the UAV as compared the scenario in which the UAV is behind or above it. If the UAV-to-user channel is assumed to follow a free-space path-loss model[4] *i.e.*, with channel gain between UAV i to user j modeled as $g_{i,j} = \frac{\beta}{d_{i,j}^2}$ (assuming the probability of a LoS channel as 1 for rural area [53]), where β is the channel power gain at the reference distance 1 m, and $d_{i,j}$ is the link distance, the sum ergodic secrecy rate for configuration 1 or 2 is maximum if UAVs 1 and 2 are positioned at (10, 60) and (10, 100), respectively. However, positioning the UAVs 1 and 2 at (10, 60) and (10, 100), respectively, would result in a poor ergodic secrecy rate for users 1 and 2, as shown in Tables V–VIII. It can be observed from Tables V and VI that the optimal locations of UAVs 1 and 2 for configuration 1 that maximizes the sum ergodic secrecy rate are (10, 80) m and (30, 20) m, respectively, for which the sum ergodic rate is 16.38 bps/Hz. It can be observed from Tables VII and VIII that the optimal locations of UAVs 1 and 2 for configuration 2 are (10, 20) m and (20, 60) m, respectively, for which sum ergodic rate is 9.9 bps/Hz. The change in the optimal location of both UAVs due to the discussed human-induced effects are shown in Fig. 13(c). We then conclude that positioning UAVs using the knowledge of human body orientation and human body effects on wireless channels when UAVs are flying at low altitudes results in a significantly higher ergodic secrecy rate compared to the UAVs' location optimization strategies that are employed without considering the human-induced effects.

machine learning methods, such as [43] or using an optical camera if available. Using this information and (7), the ergodic rate lookup tables, such as Tables V–VIII, can be generated.

[4]Free-space path-loss models have been commonly adopted by the UAV research community to model the UAV-to-user channel [53]–[55].

IX. CONCLUSION

We have experimentally shown how the human body and different use cases of holding a UE can affect the LOS UAV-to-Ground channel at ultra-low altitudes. First, compared to a scenario where the receiver node is mounted on a tripod in free space, the human body is shown to result in gains/losses depending on the user's orientation relative to the transmitting UAV. Second, we show that, depending on the drone's hovering position, there are two distinct regions for shadowing and multipath: One that is dominated by the drone body and another that is strongly dependent on the user's orientation. Multipath effects, for instance, are shown to reduce by 50% as the UAV moves from directly above the user to more-distant locations that have better Tx-Rx path clearance. Fourth, we show that the near-body location of the UE and user orientation can have a considerable impact on the wireless channel. This impact, however, can strongly depend on the drone's hovering position, as improvements in channel quality could be achieved by simply readjusting the drone's altitude. After addressing the time-varying nature of the K-factor as a result of UAV hovering, we show that the Rician K-factor is not only a function of altitude, but can strongly depend on user orientation with reductions in the average value reaching 15 dB at some drone hovering

locations. A frequency comparison is then performed revealing that the 900 MHz frequency results in a higher K-factor across all use cases. Finally, to demonstrate the impact of our findings on real-world applications, we consider how the observed human and UAV body induced effects can influence the physical layer security in a UAV-assisted network. We have shown that deciding UAVs' hovering locations considering the ground user's body and their orientation result in significant improvements in ergodic secrecy rate compared to the traditional physical layer security schemes that employ free-space pathloss model for the AtG channels and neglect the human-induced effects.

REFERENCES

[1] M. Badi, D. Rajan, and J. Camp, "Measurement-based characterization of the human body impact on ultra-low UAV-to-ground channels," *Proc. IEEE Military Commun. Conf. (MILCOM)*, Dec. 2021.

[2] Drones for Disaster response: NASA STEReO project kicks off, 2020. [Online]. Available: https://www.nasa.gov/feature/ames/drones-for-disasterresponse-nasa-stereo-project-kicks-off

[3] Y. Zeng, R. Zhang, and T. J. Lim, "Wireless communications with unmanned aerial vehicles: Opportunities and challenges," *IEEE Commun. Mag.*, vol. 54, no. 5, pp. 36–42, May 2016.

[4] "Global Drone Market Report 2021-2026, New insights on the commercial drone market and an updated model for the drone market report," *Drone Ind. Insights*, [Online]. Available : https://droneii.com/product/drone-market-report.

[5] Internet-of-things driving wireless technologies, Keysight Technologies, [Online]. Available: https://www.keysight.com/us/en/assets/7018-05035/posters/5992-1217.pdf.

[6] *Federal Communications Commission fact sheet*, *Transitioning the 900 MHz band to enable broadband deployment*. [Online]. Available: https://docs.fcc.gov/public/attachments/DOC-363915A1.pdf.

[7] V. Plicanic, B. K. Lau, A. Derneryd, and Z. Ying, "Actual diversity performance of a multiband diversity antenna with hand and head effects," *IEEE Trans. Antennas Propag.*, vol. 57, no. 5, pp. 1547–1556, May 2009.

[8] Y. Shi, J. Wensowitch, E. Johnson, and J. Camp, "A measurement study of user-induced propagation effects for UHF frequency bands," in *Proc. IEEE SECON*, 2017, pp. 1–9.

[9] Ł. Januszkiewicz, "Analysis of human body shadowing effect on wireless sensor networks operating in the 2.4 GHz band," *Sensors*, vol. 18, no. 10, 2018.

[10] B. Kibret, A. K. Teshome, and D. T. H. Lai, "Characterizing the human body as a monopole antenna," *IEEE Trans. Antennas Propag.*, vol. 63, no. 10, pp. 4384–4392, Oct. 2015

[11] G. Cohn, D. Morris, S. N. Patel, and D. S. Tan, "Your noise is my command: Sensing gestures using the body as an antenna," in *Proc. ACM Conf. Human Factors Comput. Syst.*, 2011, pp. 791–800.

[12] N. Amani, V. Dehghanian, and J. Nielsen, "User-induced antenna variation and its impact on the performance of RSS-based indoor positioning," in *Proc. IEEE Can. Conf. Elect. Comput. Eng.*, Vancouver, BC, Canada, 2016, pp. 1–5

[13] M. M. Khan, "Comprehensive study of on-body radio channels at 2.45 GHz for different human test subjects," in *Proc. Intern. Conf. Elect. Eng. Info. Commun. Tech.*, 2014, pp. 1–5.

[14] S. Shikhantsov *et al.*, "Massive MIMO propagation modeling with user-induced coupling effects using ray-tracing and FDTD," *IEEE J. Sel. Areas Commun.*, vol. 38, no. 9, pp. 1955–1963, Sep. 2020.

[15] M. Heino, C. Icheln, and K. Haneda, "Self-user shadowing effects of millimeter-wave mobile phone antennas in a browsing mode," in *Proc. 13th Eur. Conf. Antennas Propag.*, 2019, pp. 1–5.

[16] M. Mohamed, M. Cheffena, A. Moldsvor, and F. P. Fontan, "Physical statistical channel model for off-body area network," *IEEE Antennas Wireless Propag. Lett.*, vol. 16, pp. 1516–1519, 2017.

[17] S. Cotton, A. McKernan, A. Ali, and W. Scanlon, "An experimental study on the impact of human body shadowing in off-body communications channels at 2.45 GHz," in *Proc. 5th Eur. Conf. Antennas Propag.*, 2011, pp. 3133–3137.

[18] I. Dove, "Analysis of radio propagation inside the human body for in-body localization purposes," Master's Thesis, University of Twente, Enschede, The Netherlands, Aug. 2014.

[19] C. W. Kim and T. S. P. See, "RF transmission power loss variation with abdominal tissues thicknesses for ingestible source," in *Proc. IEEE Int. Conf. 13th e-Health Netw. Appl. Serv.*, 2011, pp. 282–287.

[20] F. D. Rosa, M. Pelosi, and J. Nurmi, "Human-induced effects on RSS ranging measurements for cooperative positioning," *Hindawi Int. J. Navig. Observation*, vol. 2012, pp. 1–13, Nov. 2012.

[21] E. Cabot, I. Stevanovic, N. Kuster, and M. H. Capstick, "A numerical assessment of the human body effect in the transmission of wireless microphones," *Microwave Optical Technol. Letters*, vol. 61, no. 3, pp. 809–817, Mar. 2019. [Online]. Available: https://d24z4d3zypmncx.cloudfront.net/KnowledgeBaseFiles/effect_human_body_wireless_mic_transmission.pdf

[22] Y. Ma, Z. Luo, C. Steiger, G. Traverso, and F. Adib, "Enabling deep-tissue networking for miniature medical devices," in *Proc. ACM SIGCOMM Conf.*, New York, NY, USA, 2018, pp. 417–431.

[23] A. Thielens *et al.*, *A Comparative Study of On-Body Radio-Frequency Links in the 420 MHz-2.4 GHz Range. Sensors*, 2018, vol. 18, 4165. [Online]. Available: https://doi.org/10.3390/s18124165

[24] P. A. Catherwood *et al.*, "Radio channel characterization of mid-band 5G service delivery for ultra-low altitude aerial base stations," *IEEE Access* vol. 7, pp. 8283–8299, Jan. 2019.

[25] L. Ferranti, L. Bonati, S. D'Oro, and T. Melodia, "SkyCell: A prototyping platform for 5G aerial base stations," in *Proc. IEEE WoWMoM*, 2020, pp. 329–334.

[26] Y. Shi, R. Enami, J. Wensowitch, and J. Camp, "Measurement-based characterization of LOS and NLOS drone-to-ground channels," in *Proc. IEEE WCNC - PHY Fundamentals*, Barcelona, Spain, 2018, pp. 1–6.

[27] S. Mohanti *et al.*, "AirBeam: Experimental demonstration of distributed beamforming by a swarm of UAVs," in *Proc. IEEE MASS*, Monterey, CA, USA, 2019, pp. 162–170

[28] W. Khawaja, O. Ozdemir, and I. Guvenc, "UAV air-to-ground channel characterization for mmWave systems," in *Proc. IEEE VTC - Fall Workshops*, 2017, pp. 1–5.

[29] M. Badi, J. Wensowitch, D. Rajan, and J. Camp, "Experimentally analyzing diverse antenna placements and orientations for UAV communications," *IEEE Trans. Veh. Technol.*, vol. 69, no. 12, pp. 14989–15004, Dec. 2020

[30] M. Simunek, F. P. Fontan, and P. Pechac, "The UAV low elevation propagation channel in urban areas: Statistical analysis and time-series generator," *IEEE Trans. Antennas Propag.*, vol. 61, no. 7, pp. 3850–3858, Jul. 2013

[31] J. Rodríguez-Piñeiro, T. Domínguez-Bolaño, X. Cai, Z. Huang, and X. Yin, "Air-to-ground channel characterization for low-height UAVs in realistic network deployments," *IEEE Trans. Antennas Prop.*, vol. 69, no. 2, pp. 992–1006, Feb. 2021.

[32] T. Choi *et al.*, "Using a drone sounder to measure channels for cell-free massive MIMO systems," 2021. [Online]. Available: https://arxiv.org/abs/2106.15276

[33] R. Gangula, O. Esrafilian, D. Gesbert, C. Roux, F. Kaltenberger, and R. Knopp, "Flying rebots: First results on an autonomous UAV-Based LTE relay using open airinterface," in *Proc. IEEE 21st Int. Workshop Signal Process. Adv. Wirel. Commun.*, 2018, pp. 1–5.

[34] Z. Cui, C. Briso-Rodríguez, K. Guan, I. Guvenc, and Z. Zhong, "Wideband air-to-ground channel characterization for multiple propagation environments," *IEEE Antennas Wireless Propag. Lett.*, vol. 19, no. 9, pp. 1634–1638, Sep. 2020

[35] Z. Cui *et al.*, "Low-altitude UAV air-ground propagation channel measurement and analysis in a suburban environment at 3.9 GHz," *IET Microw., Antennas Propag.*, vol. 13, no. 9, pp. 1503–1508, Jul. 2019

[36] C. Briso, C. Calvo, Z. Cui, L. Zhang, and Y. Xu, "Propagation measurements and modeling for low altitude UAVs from 1 to 24 GHz," *IEEE Trans. Veh. Technol.*, vol. 69, no. 3, pp. 3439–3443, Mar. 2020

[37] N. Goddemeier and C. Wietfeld, "Investigation of air-to-air channel characteristics and a UAV specific extension to the rice model," in *Proc. IEEE Globecom (GC Workshop)*, 2015, pp. 1–5.

[38] Q. Wu, J. Xu, and R. Zhang, "Capacity characterization of UAV-enabled two-user broadcast channel," *IEEE J. Sel. Areas Commun.*, vol. 36, no. 9, pp. 1955–1971, Sep. 2018

[39] Z. Wang, L. Duan, and R. Zhang, "Adaptive deployment for UAV-aided communication networks," *IEEE Trans. Wireless Commun.*, vol. 18, no. 9, pp. 4531–4543, Sep. 2019

[40] B. Li, S. Zhao, R. Zhang, H. Zhang, H. Wang, and L. Yang, "Joint transmit power and trajectory optimization for two-way multi-hop UAV relaying networks," in *Proc. IEEE Int. Conf. Commun. (Workshops)*, 2020, pp. 1–5.

[41] S. Ahmed, M. Z. Chowdhury, and Y. M. Jang, "Energy-efficient UAV-to-user scheduling to maximize throughput in wireless networks," *IEEE Access*, vol. 8, pp. 21215–21225, 2020.
[42] J. Guo, P. Walk, and H. Jafarkhani, "Optimal deployments of UAVs with directional antennas for a power-efficient coverage," *IEEE Trans. Commun.*, vol. 68, no. 8, pp. 5159–5174, Aug. 2020
[43] L. Zhang, Y. Hua, S. L. Cotton, S. K. Yoo, C. R. C. M. Da Silva, and W. G. Scanlon, "An RSS-based classification of user equipment usage in indoor millimeter wave wireless networks using machine learning," *IEEE Access*, vol. 8, pp. 14928–14943, 2020
[44] J. Zhang, K. Tan, J. Zhao, H. Wu, and Y. Zhang, "A practical SNR guided rate adaptation," in *Proc. IEEE INFOCOM*, 2008, pp. 2083–2091.
[45] T. Watteyne, S. Lanzisera, A. Mehta, and K. Pister, "Mitigating multipath fading through channel hopping in wireless sensor networks," in *Proc. IEEE Int. Conf. Commun*., 2010, pp. 1–5.
[46] A. Goldsmith, *Wireless Communications*. Cambridge, U.K.: Cambridge Univ. Press, 2005.
[47] L. J. Greenstein, D. G. Michelson, and V. Erceg, "Moment-method estimation of the ricean k-factor," *IEEE Commun. Lett.*, vol. 3, no. 6, pp. 175–176, Jun. 1999
[48] VERT2450 Antenna Data-sheet, Ettus Research LLC, and anechoic chamber measurements results for co-polarized and cross-polarized links in the elevation and azimuth planes. [Online]. Available: https://smu.box.com/s/wnmq2xf8fiefd5pwse88w60an8vy7jmm
[49] C. Balanis, *Antenna Theory, Analysis, and Design*, 2nd ed. New York, NY, USA: Wiley, 1997.
[50] F.1336: Reference radiation patterns of omnidirectional, sectoral and other antennas for the fixed and mobile service for use in sharing studies in the frequency range from 400 MHz to about 70 GHz. [Online]. Available: https://www.itu.int/rec/R-REC-F.1336/en
[51] P. Sundaram, D. Matolak, and D. Irwin, "New results for characterization of indoor channels in two ISM bands (900-928 MHZ and 2.4-2.5 GHz)," M.S. Thesis, Mar. 2006. [Online]. Available: https://etd.ohiolink.edu/apexprod/rws_etd/send_file/send?accession=ohiou1140462634&disposition=attachment
[52] P. K. Gopala, L. Lai, and H. El Gamal, "On the secrecy capacity of fading channels," *IEEE Trans. Inf. Theory*, vol. 54, no. 10, pp. 4687–4698, Oct. 2008.
[53] L. Xiao, Y. Xu, D. Yang and Y. Zeng, "Secrecy energy efficiency maximization for UAV-enabled mobile relaying," *IEEE Trans. Green Commun. Netw.*, vol. 4, no. 1, pp. 180–193, Mar. 2020.
[54] B. Duo, Q. Wu, X. Yuan, and R. Zhang, "Energy efficiency maximization for full-duplex UAV secrecy communication," *IEEE Trans. Veh. Technol.*, vol. 69, no. 4, pp. 4590–4595, Apr. 2020.
[55] Y. Zhou, C. Pan, P. L. Yeoh, K. W. M. Elkashlan, B. Vucetic, and Y. Li, "Secure communications for UAV-enabled mobile edge computing systems," *IEEE Trans. Commun.*, vol. 68, no. 1, pp. 376–388, Jan. 2020.
[56] M. Fernandez, L. Zhang, S. Cotton and D. Guerra, "Path loss measurements of user equipment to access point communications at 60 GHz" in *Proc. IEEE Int. Symp. Broadband Multimedia Syst. Broadcast.*, 2020, pp. 1–5.

Mahmoud Badi received the B.S. degree in electrical and electronics engineering from the University of Tripoli, Libya, in 2012, and the M.S. degree in 2017 in telecommunications through the Fulbright Foreign Student Program Scholarship from Southern Methodist University, Dallas, TX, USA, where he is currently working toward Ph.D. degree in electrical and computer engineering. His current research interests include UAV communications, centralized and distributed multiple antenna systems, and off-body communications.

Sabyasachi Gupta received the M.Tech. degree from the National Institute of Technology, Durgapur, India, and the Ph.D. degree from the Indian Institute of Technology Delhi, New Delhi, India. He has held a Research positions with the University of Pompeu Fabra, Barcelona, Spain, and with the University of Alabama, Tuscaloosa, AL, USA. He is currently a Postdoctoral Fellow with the Department of Electrical and Computer Engineering, Southern Methodist University, Dallas, TX, USA. His research interests include resource allocation for wireless networks, mobile-edge computing networks, investigating application of optimization technique, machine learning, and graph theory for wireless communication. He was the recipient of the Institute Gold Medal from NIT Durgapur in 2010.

Dinesh Rajan (Senior Member, IEEE) received the B.Tech. degree in electrical engineering from the Indian Institute of Technology Madras, Chennai, India, and the M.S. and Ph.D. degrees in electrical and computer engineering from Rice University, Houston, TX, USA. He is currently the Department Chair and Cecil and Ida Green Professor with Electrical and Computer Engineering Department, Southern Methodist University, Dallas, TX, USA. In August 2002, he joined the Electrical Engineering Department, Southern Methodist University, Dallas, TX, USA, as an Assistant Professor. His current research interests include communications theory, wireless networks, information theory and computational imaging. He was the recipient of the NSF CAREER Award for his work on applying information theory to the design of mobile wireless networks. He was also the recipient of the Golden Mustang Outstanding Faculty Award and the Senior Ford Research Fellowship from SMU.

Joseph Camp (Member, IEEE) received the B.S. (Hons.) degree in electrical and computer engineering from The University of Texas at Austin, Austin, TX, USA, and the M.S. and Ph.D. degrees in electrical and computer engineering from Rice University, Houston, TX, USA. He is currently an Associate Professor of electrical and computer engineering with Southern Methodist University, Dallas, TX, USA. In 2009, he joined the SMU Faculty. His research team has performed more than 200 million in-field wireless measurements around the world via Android deployment and local characterization via drones, campus buses, vehicles, and buildings. His research interests include wireless communications and networking, crowdsourcing, and drones, specifically focused on the deployment, measurement, and analysis of large-scale systems and development of embedded protocols. He was the recipient of the Ralph Budd Award for the best engineering thesis at Rice University (2010), the National Science Foundation CAREER Award (2012), the Golden Mustang Teaching Award (2014), and the Gerald J. Ford Research Fellowship (2021).